

# Gamma-Ray Bursts: The Underlying Model

Eli Waxman

Weizmann Institute of Science, Rehovot 76100, Israel

**Abstract.** A pedagogical derivation is presented of the “fireball” model of  $\gamma$ -ray bursts, according to which the observable effects are due to the dissipation of the kinetic energy of a relativistically expanding wind, a “fireball.” The main open questions are emphasized, and key afterglow observations, that provide support for this model, are briefly discussed. The relativistic outflow is, most likely, driven by the accretion of a fraction of a solar mass onto a newly born (few) solar mass black hole. The observed radiation is produced once the plasma has expanded to a scale much larger than that of the underlying “engine,” and is therefore largely independent of the details of the progenitor, whose gravitational collapse leads to fireball formation. Several progenitor scenarios, and the prospects for discrimination among them using future observations, are discussed. The production in  $\gamma$ -ray burst fireballs of high energy protons and neutrinos, and the implications of burst neutrino detection by kilometer-scale telescopes under construction, are briefly discussed.

## 1 Introduction

The widely accepted interpretation of the phenomenology of  $\gamma$ -ray bursts (GRBs), of 0.1 – 1 MeV photons lasting for a few seconds (see [39] for a review), is that the observable effects are due to the dissipation of the kinetic energy of a relativistically expanding wind, a “fireball,” whose primal cause is not yet known. The recent detection of “afterglows,” delayed low energy (X-ray to radio) emission of GRBs (see [69] for a review), confirmed the cosmological origin of the bursts through the redshift determination of several GRB host-galaxies, and supported standard model predictions of afterglows that result from the collision of an expanding fireball with its surrounding medium (see [78,92] for reviews).

The fireball model is described in §§ 2, 3, and 4 of this chapter. The phenomenological arguments suggesting that fireball formation is likely regardless of the underlying progenitor are presented, and fireball hydrodynamics and radiative processes are discussed in detail in §§2 and 3, respectively. The main open questions related to fireball physics are discussed in §3.4. Since both the theory and the implications of afterglow observations are extensively discussed in other chapters of this volume, we include in §4 of this chapter only a brief discussion of several key afterglow implications. We also limit the theoretical discussion of fireball evolution to the GRB production phase that precedes the afterglow phase during which evolution is dominated by the interaction of the fireball with its surrounding medium. We do discuss, however, the initial non-self-similar onset of this interaction, which marks the onset of the afterglow phase.

The GRB progenitors are not yet known. We present in §5 the constraints imposed by observations on possible progenitors, and discuss the (presently) leading candidates. Hints provided by afterglow observations, which are extensively discussed in separate chapters of this volume, are briefly reviewed.

The association of GRBs with ultra-high energy cosmic-rays (UHECR), the evidence for which is strengthened by recent afterglow observations, is based on two key points [115]: 1) the constraints that a dissipative ultra-relativistic wind must satisfy in order to allow acceleration of protons to energy  $\sim 10^{20}$  eV, the highest observed cosmic-ray energy, are remarkably similar to the constraints imposed on the fireball wind by  $\gamma$ -ray observations, and 2) the inferred local ( $z = 0$ ) GRB energy generation rate of  $\gamma$ -rays is remarkably similar to the local generation rate of UHECR implied by cosmic-ray observations. We briefly discuss in §6 production of high energy protons and neutrinos in GRB fireballs (see [120,121] for more detailed reviews). The GRB model for UHECR production makes unique predictions that may be tested with operating and planned large area UHECR detectors [27,29,106,114]<sup>1</sup>. In this review we focus, however, on more recent predictions of neutrino emission, which may be tested with planned high energy neutrino telescopes [57]. Detection of the predicted neutrino signal will confirm the GRB fireball model for the production of UHECR and may allow discrimination between different fireball progenitor scenarios. Moreover, a detection of even a handful of neutrino events correlated with GRBs will allow a test for neutrino properties, e.g., flavor oscillation and coupling to gravity, with accuracy many orders of magnitude better than currently possible.

## 2 The Fireball Model: Hydrodynamics

### 2.1 Relativistic Expansion

General phenomenological considerations, based on  $\gamma$ -ray observations, indicate that, regardless of the nature of the underlying sources, GRBs are produced by the dissipation of the kinetic energy of a relativistically expanding fireball. The rapid rise time and short duration,  $\sim 1$  ms, observed in some bursts [13,38] imply that the sources are compact, with a linear scale comparable to a light-ms,  $r_0 \sim 10^7$  cm. The high  $\gamma$ -ray luminosity implied by cosmological distances,  $L_\gamma \sim 10^{52}$  erg s<sup>-1</sup>, then results in a very high optical depth to pair creation since the energy of observed  $\gamma$ -ray photons is above the threshold for pair production. The number density of photons at the source  $n_\gamma$  is approximately given by

$$L_\gamma = 4\pi r_0^2 c n_\gamma \epsilon, \quad (1)$$

where  $\epsilon \simeq 1$  MeV is the characteristic photon energy. Using  $r_0 \sim 10^7$  cm, the optical depth for pair production at the source is

<sup>1</sup> See also <http://www.physics.adelaide.edu.au/astrophysics/FlysEye.html>, <http://www-ta.icrr.u-tokyo.ac.jp/>, and <http://www.auger.org/>

$$\tau_{\gamma\gamma} \sim r_0 n_\gamma \sigma_T \sim \frac{\sigma_T L_\gamma}{4\pi r_0 c \epsilon} \sim 10^{15}, \quad (2)$$

where  $\sigma_T$  is the Thomson cross section.

The high optical depth implies that a thermal plasma of photons, electrons, and positrons is created, a fireball which then expands and accelerates to relativistic velocities [50,87]. The optical depth is reduced by relativistic expansion of the source. If the source expands with a Lorentz factor  $\Gamma$ , the energy of photons in the source frame is smaller by a factor  $\Gamma$  compared to that in the observer frame, and most photons may therefore be below the pair production threshold.

A lower limit for  $\Gamma$  may be obtained in the following way [10,67]. The GRB photon spectrum is well fitted in the *Burst and Transient Source Experiment (BATSE)* detectors range, 20 keV to 2 MeV [39], by a combination of two power-laws,  $dn_\gamma/d\epsilon_\gamma \propto \epsilon_\gamma^{(\alpha-1)}$  ( $\alpha$  is the flux density spectral index,  $F_\nu \propto \nu^{+\alpha}$ ) with different values of  $\alpha$  at low and high energy [9]. Here,  $dn_\gamma/d\epsilon_\gamma$  is the number of photons per unit photon energy. The break energy (where  $\alpha$  changes) in the observer frame is typically  $\epsilon_{\gamma b} \sim 1$  MeV, with  $\alpha \simeq 0$  at energies below the break and  $\alpha \simeq -1$  above the break. In several cases, the spectrum has been observed to extend to energies  $> 100$  MeV [39,103]. Consider then a high energy test photon, with observed energy  $\epsilon_t$ , trying to escape the relativistically expanding source. Assuming that, in the source rest frame, the photon distribution is isotropic, and that the spectrum of high energy photons follows  $dn_\gamma/d\epsilon_\gamma \propto \epsilon_\gamma^{-2}$ , the mean free path for pair production (in the source rest frame) for a photon of energy  $\epsilon'_t = \epsilon_t/\gamma$  (in the source rest frame) is

$$l_{\gamma\gamma}^{-1}(\epsilon'_t) = \frac{1}{2} \frac{3}{16} \sigma_T \int d\cos\theta (1 - \cos\theta) \int_{\epsilon_{\text{th}}(\epsilon'_t, \theta)}^{\infty} d\epsilon \frac{U_\gamma}{2\epsilon^2} = \frac{1}{16} \sigma_T \frac{U_\gamma \epsilon'_t}{(m_e c^2)^2}. \quad (3)$$

Here,  $\epsilon_{\text{th}}(\epsilon'_t, \theta)$  is the minimum energy of photons that may produce pairs interacting with the test photon, given by  $\epsilon_{\text{th}} \epsilon'_t (1 - \cos\theta) \geq 2(m_e c^2)^2$  ( $\theta$  is the angle between the photons' momentum vectors).  $U_\gamma$  is the photon energy density (in the range corresponding to the observed *BATSE* range) in the source rest-frame, given by

$$L_\gamma = 4\pi r^2 \gamma^2 c U_\gamma. \quad (4)$$

(Note that we have used a constant cross section,  $3\sigma_T/16$ , above the threshold  $\epsilon_{\text{th}}$ .) The cross section drops as  $\log(\epsilon)/\epsilon$  for  $\epsilon \gg \epsilon_{\text{th}}$ ; however, since the number density of photons drops rapidly with energy, this does not introduce a large correction to  $l_{\gamma\gamma}$ .

The source size constraint implied by the variability time is modified for a relativistically expanding source. Since in the observer frame almost all photons propagate at a direction making an angle  $< 1/\Gamma$  with respect to the expansion direction, radiation seen by a distant observer originates from a conical section of the source around the source-observer line of sight, with opening angle  $\sim 1/\Gamma$ . Photons which are emitted from the edge of the cone are delayed, compared to

those emitted on the line of sight, by  $r/2\Gamma^2c$ . Thus, the constraint on source size implied by variability on time scale  $\Delta t$  is

$$r \sim 2\Gamma^2c\Delta t. \quad (5)$$

The time  $r/c$  required for significant source expansion corresponds to comoving time (measured in the source frame)  $t_{\text{co.}} \approx r/\Gamma c$ . The two-photon collision rate at the source frame is  $t_{\gamma\gamma}^{-1} = c/l_{\gamma\gamma}$ . Thus, the source optical depth to pair production is  $\tau_{\gamma\gamma} = t_{\text{co.}}/t_{\gamma\gamma} \approx r/\Gamma l_{\gamma\gamma}$ . Using Eqs. (3) and (5) we have

$$\tau_{\gamma\gamma} = \frac{1}{128\pi} \frac{\sigma_T L_\gamma \epsilon_t}{c^2 (m_e c^2)^2 \Gamma^6 \Delta t}. \quad (6)$$

Requiring  $\tau_{\gamma\gamma} < 1$  at  $\epsilon_t$  we obtain a lower limit for  $\Gamma$ ,

$$\Gamma \geq 250 \left[ L_{\gamma,52} \left( \frac{\epsilon_t}{100\text{MeV}} \right) \Delta t_{-2}^{-1} \right]^{1/6}, \quad (7)$$

where  $L_\gamma = 10^{52} L_{\gamma,52} \text{ erg s}^{-1}$  and  $\Delta t = 10^{-2} \Delta t_{-2} \text{ s}$ .

## 2.2 Fireball Evolution

As the fireball expands it cools, the photon temperature  $T_\gamma$  in the fireball frame decreases, and most pairs annihilate. Once the pair density is sufficiently low, photons may escape. However, if the observed radiation is due to photons escaping the fireball as it becomes optically thin, two problems arise. First, the photon spectrum is quasi-thermal, in conflict with observations. Second, the source size,  $r_0 \sim 10^7 \text{ cm}$ , and the total energy emitted in  $\gamma$ -rays,  $\sim 10^{53} \text{ erg}$ , suggest that the underlying energy source is related to the gravitational collapse of a  $\sim 1 M_\odot$  object. Thus, the plasma is expected to be loaded with baryons which may be injected with the radiation or present in the atmosphere surrounding the source. A small baryonic load,  $\geq 10^{-8} M_\odot$ , increases the optical depth due to Thomson scattering on electrons associated with the loading protons, so that most of the radiation energy is converted to kinetic energy of the relativistically expanding baryons before the plasma becomes optically thin [88,102]. To overcome both problems it was proposed [95] that the observed burst is produced once the kinetic energy of the ultra-relativistic ejecta is re-randomized by some dissipation process at large radius, beyond the Thomson photosphere, and then radiated as  $\gamma$ -rays. Collision of the relativistic baryons with the interstellar medium (ISM) [95], and internal collisions within the ejecta itself [79,86,91], were proposed as possible dissipation processes. Most GRBs show variability on time scales much shorter (typically  $10^{-2}$  times) than the total GRB duration. Such variability is hard to explain in models where the energy dissipation is due to external shocks [98,127]. Thus, it is believed that internal collisions are responsible for the emission of  $\gamma$ -rays.

Let us first consider the case where the energy release from the source is ‘‘instantaneous,’’ i.e., on a time scale of  $r_0/c$ . We assume that most of the energy is released in the form of photons, i.e., that the fraction of energy carried by

baryon rest mass  $M$  satisfies  $\eta^{-1} \equiv Mc^2/E \ll 1$ . The initial thickness of the fireball shell is  $r_0$ . Since the plasma accelerates to relativistic velocity, all fluid elements move with velocity close to  $c$ , and the shell thickness remains constant at  $r_0$  (this changes at very late time, as discussed below). We are interested in the stage where the optical depth (due to pairs and/or electrons associated with baryons) is high, but only a small fraction of the energy is carried by pairs.

The entropy of a fluid component with zero chemical potential is  $S = V(e + p)/T$ , where  $e$ ,  $p$  and  $V$  are the (rest frame) energy density, pressure and volume. For the photons  $p = e/3 \propto T_\gamma^4$ . Since initially both the rest mass and thermal energy of baryons is negligible, the entropy is provided by the photons. Conservation of entropy implies

$$r^2 \Gamma(r) r_0 T_\gamma^3(r) = \text{const}, \quad (8)$$

and conservation of energy implies

$$r^2 \Gamma(r) r_0 \Gamma(r) T_\gamma^4(r) = \text{const}. \quad (9)$$

Here  $\Gamma(r)$  is the shell Lorentz factor. Combining (8) and (9) we find

$$\Gamma(r) \propto r, \quad T_\gamma \propto r^{-1}, \quad n \propto r^{-3}, \quad (10)$$

where  $n$  is the rest frame (comoving) baryon number density.

As the shell accelerates the baryon kinetic energy,  $\Gamma M c^2$ , increases. It becomes comparable to the total fireball energy when  $\Gamma \sim \eta$ , at radius  $r_f = \eta r_0$ . At this radius most of the energy of the fireball is carried by the baryon kinetic energy, and the shell does not accelerate further. Eq. (9) describing energy conservation is replaced with  $\Gamma = \text{const}$ . Eq. (8), however, still holds. Eq. (8) may be written as  $T_\gamma^4/nT_\gamma = \text{const}$  (constant entropy per baryon). This implies that the ratio of radiation energy density to thermal energy density associated with the baryons is  $r$  independent. Thus, the thermal energy associated with the baryons may be neglected at all times, and Eq. (8) holds also for the stage where most of the fireball energy is carried by the baryon kinetic energy. Thus, for  $r > r_f$  we have

$$\Gamma(r) = \Gamma \approx \eta, \quad T \propto r^{-2/3}, \quad n \propto r^{-2}. \quad (11)$$

Let us consider now the case of extended emission from the source, on time scale  $\gg r_0/c$ . In this case, the source continuously emits energy at a rate  $L$ , and the energy emission is accompanied by mass-loss rate

$$\dot{M} = L/\eta c^2. \quad (12)$$

For  $r < r_f$  the fluid energy density is relativistic,  $aT_\gamma^4/nm_p c^2 = \eta r_0/r$ , and the speed of sound is  $\sim c$ . The time it takes the shell at radius  $r$  to expand significantly is  $r/c$  in the observer frame, corresponding to  $t_{\text{co}} \sim r/\Gamma c$  in the shell frame. During this time sound waves can travel a distance  $cr/\Gamma c$  in the shell frame, corresponding to  $r/\Gamma^2 = r/(r/r_0)^2 = (r_0/r)r_0$  in the observer frame. This

implies that at the early stages of evolution,  $r \sim r_0$ , sound waves had enough time to smooth out spatial fluctuations in the fireball over a scale  $r_0$ , but that regions separated by  $\Delta r > r_0$  cannot interact with each other. Thus, if the emission extends over a time  $t_{\text{GRB}} \gg r_0/c$ , a fireball of thickness  $ct_{\text{GRB}} \gg r_0$  would be formed, which would expand as a collection of independent, roughly uniform, sub-shells of thickness  $r_0$ . Each sub-shell would reach a final Lorentz factor  $\Gamma_f$ , which may vary between sub-shells. This implies that different sub-shells may have velocities differing by  $\Delta v \sim c/2\eta^2$ , where  $\eta$  is some typical value representative of the entire fireball. Different shells emitted at times differing by  $\Delta t$ ,  $r_0/c < \Delta t < t_{\text{GRB}}$ , may therefore collide with each other after a time  $t_c \sim c\Delta t/\Delta v$ , i.e., at a radius

$$r_i \approx 2\Gamma^2 c\Delta t = 6 \times 10^{13} \Gamma_{2.5}^2 \Delta t_{-2} \text{ cm}, \quad (13)$$

where  $\Gamma = 10^{2.5} \Gamma_{2.5}$ . The minimum internal shock radius,  $r \sim \Gamma^2 r_0$ , is also the radius at which an individual sub-shell may experience significant change in its width  $r_0$ , due to Lorentz factor variation across the shell.

### 2.3 The Allowed Range of Lorentz Factors and Baryon Loading

The acceleration,  $\Gamma \propto r$ , of fireball plasma is driven by radiation pressure. Fireball protons are accelerated through their coupling to the electrons, which are coupled to fireball photons. We have assumed in the analysis presented above, that photons and electrons are coupled throughout the acceleration phase. However, if the baryon loading is too low, radiation may decouple from fireball electrons already at  $r < r_f$ . The fireball Thomson optical depth is given by the product of comoving expansion time,  $r/\Gamma(r)c$ , and the photon Thomson scattering rate,  $n_e c\sigma_T$ . The electron and proton comoving number densities are equal,  $n_e = n_p$ , and are determined by equating the  $r$  independent mass flux carried by the wind,  $4\pi r^2 c\Gamma(r)n_p m_p$ , to the mass-loss rate from the underlying source, which is related to the rate  $L$  at which energy is emitted through  $\dot{M} = L/(\eta c^2)$ . Thus, during the acceleration phase,  $\Gamma(r) = r/r_0$  and the Thomson optical depth,  $\tau_T$ , is  $\tau_T \propto r^{-3}$ . The Thomson optical depth drops below unity at a radius  $r < r_f = \eta r_0$  if  $\eta > \eta_*$ , where

$$\eta_* = \left( \frac{\sigma_T L}{4\pi r_0 m_p c^3} \right)^{1/4} = 1.0 \times 10^3 L_{52}^{1/4} r_{0,7}^{-1/4}. \quad (14)$$

Here  $r_0 = 10^7 r_{0,7}$  cm.

If  $\eta > \eta_*$  radiation decouples from the fireball plasma at  $\Gamma = r/r_0 = \eta_*^{4/3} \eta^{-1/3}$ . If  $\eta \gg \eta_*$ , then most of the radiation energy is not converted to kinetic energy prior to radiation decoupling, and most of the fireball energy escapes in the form of thermal radiation. Thus, the baryon load of fireball shells, and the corresponding final Lorentz factors, must be within the range  $10^2 \leq \Gamma \approx \eta \leq \eta_* \approx 10^3$  in order to allow the production of the observed non-thermal  $\gamma$ -ray spectrum.

## 2.4 Fireball Interaction with the Surrounding Medium

As the fireball expands, it drives a relativistic shock (blastwave) into the surrounding gas, e.g., into the ISM gas if the explosion occurs within a galaxy. In what follows, we refer to the surrounding gas as ISM gas, although the gas need not necessarily be interstellar. At early times, the fireball is little affected by the interaction with the ISM. At late times, most of the fireball energy is transferred to the ISM, and the flow approaches the self-similar blastwave solution of Blandford and McKee [17]. At this stage a single shock propagates into the ISM, behind which the gas expands with Lorentz factor

$$\Gamma_{BM}(r) = \left( \frac{17E}{16\pi n m_p c^2} \right)^{1/2} r^{-3/2} = 150 \left( \frac{E_{53}}{n_0} \right)^{1/2} r_{17}^{-3/2}, \quad (15)$$

where  $E = 10^{53} E_{53}$  erg is the fireball energy,  $n = 1n_0 \text{ cm}^{-3}$  is the ISM number density, and  $r = 10^{17} r_{17}$  cm is the shell radius. The characteristic time at which radiation emitted by shocked plasma at radius  $r$  is observed by a distant observer is  $t \approx r/4\Gamma_{BM}^2 c$  [119].

The transition to self-similar expansion occurs on a time scale  $t_{SS}$  (measured in the observer frame) comparable to the longer of the two time scales set by the initial conditions: the (observer) GRB duration  $t_{GRB}$  and the (observer) time  $t_\Gamma$  at which the self-similar Lorentz factor equals the original ejecta Lorentz factor  $\Gamma$ ,  $\Gamma_{BM}(t = t_\Gamma) = \Gamma$ . Since  $t = r/4\Gamma_{BM}^2 c$ ,

$$t = \max \left[ t_{GRB}, 5 \left( \frac{E_{53}}{n_0} \right)^{1/3} \Gamma_{2.5}^{-8/3} \text{ s} \right]. \quad (16)$$

During the transition, plasma shocked by the reverse shocks expands with Lorentz factor close to that given by the self-similar solution,

$$\Gamma_{tr.} \simeq \Gamma_{BM}(t = t_{SS}) \simeq 245 \left( \frac{E_{53}}{n_0} \right)^{1/8} t_1^{-3/8}, \quad (17)$$

where  $t = 10t_1$  s. The unshocked fireball ejecta propagate at the original expansion Lorentz factor,  $\Gamma$ , and the Lorentz factor of plasma shocked by the reverse shock in the rest frame of the unshocked ejecta is  $\simeq \Gamma/\Gamma_{tr.}$ . If  $t \simeq t_{GRB} \gg t_\Gamma$  then  $\Gamma/\Gamma_{tr.} \gg 1$ , the reverse shock is relativistic, and the Lorentz factor associated with the random motion of protons in the reverse shock is  $\Gamma_p^R \simeq \Gamma/\Gamma_{tr.}$ .

If, on the other hand,  $t \simeq t_\Gamma \gg t_{GRB}$  then  $\Gamma/\Gamma_{tr.} \sim 1$ , and the reverse shock is not relativistic. Nevertheless, the following argument suggests that the reverse shock speed is not far below  $c$ , and that the protons are therefore heated to relativistic energy,  $\Gamma_p^R - 1 \simeq 1$ . The comoving time, measured in the fireball ejecta frame prior to deceleration, is  $t_{co.} \simeq r/\Gamma c$ . The expansion Lorentz factor is expected to vary across the ejecta,  $\Delta\Gamma/\Gamma \sim 1$ , due to variability of the underlying GRB source over the duration of its energy release. Such variation would lead to expansion of the ejecta, in the comoving frame, at relativistic speed. Thus, at the deceleration radius,  $t_{co.} \simeq \Gamma t$ , the ejecta width exceeds  $\simeq ct_{co.} \simeq \Gamma ct$ .

Since the reverse shock should cross the ejecta over a deceleration time scale,  $\simeq \Gamma t$ , the reverse shock speed must be close to  $c$ . We therefore conclude that the Lorentz factor associated with the random motion of protons in the reverse shock is approximately given by  $\Gamma_p^R - 1 \simeq \Gamma/\Gamma_{\text{tr}}$ , for both  $\Gamma/\Gamma_{\text{tr}} \sim 1$  and  $\Gamma/\Gamma_{\text{tr}} \gg 1$ .

Since  $t_{\text{GRB}} \sim 10$  s is typically comparable to  $t_\Gamma$ , the reverse shocks are typically expected to be mildly relativistic.

## 2.5 Fireball Geometry

We have assumed in the discussion so far that the fireball is spherically symmetric. However, a jet-like fireball behaves as if it were a conical section of a spherical fireball as long as the jet opening angle is larger than  $\Gamma^{-1}$ . This is due to the fact that the linear size of causally connected regions,  $ct_{\text{co}} \sim r/\Gamma$  in the fireball frame, corresponds to an angular size  $ct_{\text{co}}/r \sim \Gamma^{-1}$ . Moreover, due to the relativistic beaming of radiation, a distant observer cannot distinguish between a spherical fireball and a jet-like fireball, as long as the jet opening angle  $\theta > \Gamma^{-1}$ . Thus, as long as we are discussing processes that occur when the wind is ultra-relativistic,  $\Gamma \sim 300$  (prior to significant fireball deceleration by the surrounding medium), our results apply for both a spherical and a jet-like fireball. In the latter case,  $L(E)$  in our equations should be understood as the luminosity (energy) the fireball would have carried had it been spherically symmetric.

## 3 The Fireball Model: Radiative Processes

### 3.1 Gamma-Ray Emission

If the Lorentz factor variability within the wind is significant, internal shocks will reconvert a substantial part of the kinetic energy to internal energy. The internal energy may then be radiated as  $\gamma$ -rays by synchrotron and inverse Compton emission of shock-accelerated electrons. The internal shocks are expected to be mildly relativistic in the fireball rest frame, i.e., characterized by Lorentz factor  $\Gamma_i - 1 \sim$  a few. This is due to the fact that the allowed range of shell Lorentz factors is  $\sim 10^2$  to  $\sim 10^3$  (see §2.3), implying that the Lorentz factors associated with the relative velocities are not very large. Since internal shocks are mildly relativistic, we expect results related to particle acceleration in sub-relativistic shocks (see [16] for a review) to be valid for acceleration in internal shocks. In particular, electrons are expected to be accelerated to a power law energy distribution,  $dn_e/d\Gamma_e \propto \Gamma_e^{-p}$  for  $\Gamma_e > \Gamma_m$ , with  $p \simeq 2$  [5,12,18].

The minimum Lorentz factor  $\Gamma_m$  is determined by the following consideration. Protons are heated in internal shocks to random velocities (in the wind frame)  $\Gamma_p^R - 1 \approx \Gamma_i - 1 \approx 1$ . If electrons carry a fraction  $\xi_e$  of the shock internal energy, then  $\Gamma_m \approx \xi_e(m_p/m_e)$ . The characteristic frequency of synchrotron emission is determined by  $\Gamma_m$  and by the strength of the magnetic field. Assuming that a fraction  $\xi_B$  of the internal energy is carried by the magnetic field,  $4\pi r_i^2 c \Gamma^2 B^2 / 8\pi = \xi_B L_{\text{int}}$ , the characteristic observed energy of synchrotron photons,  $\epsilon_{\gamma b} = \Gamma \hbar \Gamma_m^2 e B / m_e c$ , is



$$\epsilon_{\gamma b} \approx 1 \xi_B^{1/2} \xi_e^{3/2} \frac{L_{\gamma,52}^{1/2}}{\Gamma_{2.5}^2 \Delta t_{-2}} \text{ MeV}. \quad (18)$$

In deriving Eq. (18) we have assumed that the wind luminosity carried by internal plasma energy,  $L_{\text{int.}}$ , is related to the observed  $\gamma$ -ray luminosity through  $L_{\text{int.}} = L_\gamma / \xi_e$ . This assumption is justified since the electron synchrotron cooling time is short compared to the wind expansion time (unless the equipartition fraction  $\xi_B$  is many orders of magnitude smaller than unity), and hence electrons lose all their energy radiatively. Fast electron cooling also results in a synchrotron spectrum  $dn_\gamma/d\epsilon_\gamma \propto \epsilon_\gamma^{-1-p/2} = \epsilon_\gamma^{-2}$  at  $\epsilon_\gamma > \epsilon_{\gamma b}$ , consistent with observed GRB spectra [9].

At present, there is no theory that allows the determination of the values of the equipartition fractions  $\xi_e$  and  $\xi_B$ . Eq. (18) implies that fractions not far below unity are required to account for the observed  $\gamma$ -ray emission. We note that build up of magnetic field to near equipartition by electromagnetic instabilities is expected to be a generic characteristic of collisionless shocks (see the discussion in [16] and references therein), and is inferred to occur in other systems such as in supernova remnant shocks (see, e.g., [24,60]).

### 3.2 Break Energy Distribution

The  $\gamma$ -ray break energy  $\epsilon_{\gamma b}$  of most GRBs observed by *BATSE* detectors is in the range of 100 keV to 300 keV [22]. It may appear from Eq. (18) that the clustering of break energies in this narrow energy range requires fine tuning of fireball model parameters, which should naturally produce a much wider range of break energies. This is, however, not the case [55]. Consider the dependence of  $\epsilon_{\gamma b}$  on  $\Gamma$ . The strong  $\Gamma$  dependence of the pair production optical depth, Eq. (6), implies that if the value of  $\Gamma$  is smaller than the minimum value allowed by Eq. (7), for which  $\tau_{\gamma\gamma}(\epsilon_\gamma = 100\text{MeV}) \approx 1$ , most of the high energy photons in the power-law distribution produced by synchrotron emission,  $dn_\gamma/d\epsilon_\gamma \propto \epsilon_\gamma^{-2}$ , would be converted to pairs. This would lead to high optical depth due to Thomson scattering on  $e^\pm$ , and hence to strong suppression of the emitted flux [55]. For fireball parameters such that  $\tau_{\gamma\gamma}(\epsilon_\gamma = 100\text{MeV}) \approx 1$ , the break energy implied by Eqs. (18) and (7) is

$$\epsilon_{\gamma b} \approx 1 \xi_B^{1/2} \xi_e^{3/2} \frac{L_{\gamma,52}^{1/6}}{\Delta t_{-2}^{2/3}} \text{ MeV}. \quad (19)$$

As explained in §2.3, shell Lorentz factors cannot exceed  $\eta_* \simeq 10^3$ , for which break energies in the X-ray range,  $\epsilon_{\gamma b} \sim 10$  keV, may be obtained. We note, however, that the radiative flux would be strongly suppressed in this case too [55]. If the typical  $\Gamma$  of radiation emitting shells is close to  $\eta_*$ , then the range of Lorentz factors of wind shells is narrow, which implies that only a small fraction of wind kinetic energy would be converted to internal energy which can be radiated from the fireball.

Thus, the clustering of break energies at  $\sim 1$  MeV is naturally accounted for, provided that the variability time scale satisfies  $\Delta t \leq 10^{-2}$  s, which implies an upper limit on the source size, since  $\Delta t \geq r_0/c$  (see [36,49] for alternative explanations). We note, that a large fraction of bursts detected by *BATSE* show variability on the shortest resolved time scale,  $\sim 10$  ms [127]. In addition, a natural consequence of the model is the existence of low luminosity bursts with low, 1 – 10 keV, break energies [55]. Such “X-ray bursts” may have recently been identified [64].

For internal collisions, the observed  $\gamma$ -ray variability time,  $\sim r_i/\Gamma^2 c \approx \Delta t$ , reflects the variability time of the underlying source, and the GRB duration reflects the duration over which energy is emitted from the source. Since the wind Lorentz factor is expected to fluctuate on time scales ranging from the shortest variability time  $r_0/c$  to the wind duration  $t_{\text{GRB}}$ , internal collisions will take place over a range of radii,  $r \sim \Gamma^2 r_0$  to  $r \sim \Gamma^2 c t_{\text{GRB}}$ .

### 3.3 Afterglow Emission

Let us consider the radiation emitted from the reverse shocks during the transition to self-similar expansion. The characteristic electron Lorentz factor (in the plasma rest frame) is  $\Gamma_m \simeq \xi_e (\Gamma/\Gamma_{\text{tr}}) m_p/m_e$ , where the internal energy per proton in the shocked ejecta is  $\simeq (\Gamma/\Gamma_{\text{tr}}) m_p c^2$ . The energy density  $U$  is  $E \approx 4\pi r^2 c t \Gamma_{\text{tr}}^2 U$ , and the number of radiating electrons is  $N_e \approx E/\Gamma m_p c^2$ . Using Eq. (17) and  $r = 4\Gamma_{\text{tr}}^2 c t$ , the characteristic (or peak) energy of synchrotron photons (in the observer frame) is [124]

$$\epsilon_{\gamma m} \approx \hbar \Gamma_{\text{tr}} \Gamma_m^2 \frac{eB}{m_e c} = 2\xi_{e,-1}^2 \xi_{B,-1}^{1/2} n_0^{1/2} \Gamma_{2.5}^2 \text{ eV}, \quad (20)$$

and the specific luminosity,  $L_\epsilon = dL/d\epsilon_\gamma$ , at  $\epsilon_{\gamma m}$  is

$$L_m \approx (2\pi\hbar)^{-1} \Gamma_{\text{tr}} \frac{e^3 B}{m_e c^2} N_e \approx 10^{61} \xi_{B,-1}^{1/2} E_{53}^{5/4} t_1^{-3/4} \Gamma_{2.5}^{-1} n_0^{1/4} \text{ s}^{-1}, \quad (21)$$

where  $\xi_e = 0.1\xi_{e,-1}$ , and  $\xi_B = 0.1\xi_{B,-1}$ .

Here too, we expect a power law energy distribution,  $dN_e/d\Gamma_e \propto \Gamma_e^{-p}$  for  $\Gamma_e > \Gamma_m$ , with  $p \simeq 2$ . Since the radiative cooling time of electrons in the reverse shock is long compared to the ejecta expansion time, the specific luminosity extends in this case to energy  $\epsilon_\gamma > \epsilon_{\gamma m}$  as  $L_\epsilon = L_m (\epsilon_\gamma/\epsilon_{\gamma m})^{-1/2}$ , up to photon energy  $\epsilon_{\gamma c}$ . Here  $\epsilon_{\gamma c}$  is the characteristic synchrotron frequency of electrons for which the synchrotron cooling time,  $6\pi m_e c/\sigma_T \gamma_e B^2$ , is comparable to the ejecta (rest frame) expansion time,  $\sim \Gamma_{\text{tr}} t$ . At energy  $\epsilon_\gamma > \epsilon_{\gamma c}$ ,

$$\epsilon_{\gamma c} \approx 0.1 \xi_{B,-1}^{-3/2} n_0^{-1} E_{53}^{-1/2} t_1^{-1/2} \text{ keV}, \quad (22)$$

the spectrum steepens to  $L_\epsilon \propto \epsilon_\gamma^{-1}$ .

The shock driven into the ISM continuously heats new gas, and produces relativistic electrons that may produce the delayed afterglow radiation observed

on time scales  $t \gg t_{\text{SS}}$ , typically of order days to months. As the shock wave decelerates, the emission shifts to lower frequency with time. Since afterglow emission on such long time scale is extensively discussed in other chapters of this volume, we do not discuss in detail the theory of late-time afterglow emission.

### 3.4 Open Questions: Magnetic Field and Electron Coupling

The emission of radiation in both the GRB and afterglow phases is assumed to arise from synchrotron emission of shock accelerated electrons. To match observations, the magnetic field behind the shocks must be close to equipartition and a significant fraction of the internal shock energy must be carried by electrons, that is,  $\xi_B$  and  $\xi_e$  should be close to unity, of order 10%. During the afterglow phase, shock compression of the existing ISM field yields a field many orders of magnitude smaller than needed. Thus, the magnetic field is most likely generated in, and by, the shock wave. A similar process is likely necessary to generate the field required for synchrotron emission during the GRB phase, i.e., in the internal fireball shocks. Although a magnetic field close to equipartition at the base of the wind frozen into the fireball plasma may not be many orders of magnitude below equipartition during the internal shock phase, significant amplification is nevertheless required. It is well known that near equipartition magnetic fields may be generated in collisionless shocks through the Weibel instability (see, e.g., [63,97]). However, the field is generated on microscopic, skin-depth, scale and is therefore expected to rapidly decay, unless its coherence length grows to a macroscopic scale [53,54]. The process by which such scale increase is achieved is not understood, and probably related to the process of particle acceleration [54].

In order to produce the observed spectrum during both afterglow and GRB phases, electrons must be accelerated in the collisionless shocks to a power-law distribution,  $dn_e/d\Gamma_e \propto \Gamma_e^{-p}$  with  $p \simeq 2$ . As mentioned in §3.1, such distribution is expected in the internal shocks, which are mildly relativistic. Recent numeric and analytic calculations of particle acceleration via the first order Fermi mechanism in relativistic shocks show that similar spectral indices,  $p \approx 2.2$ , are obtained for highly-relativistic shocks as well [11,65]. The derivation of electron spectral indices is based, in both the non-relativistic and relativistic cases, on a phenomenological description of electron scattering and, therefore, does not provide a complete basic principle description of the process. In particular, these calculations do not allow one to determine the fraction of energy  $\xi_e$  carried by electrons.

## 4 The Fireball Model: Key Afterglow Implications

The following point should be clarified in the context of afterglow observations – the distribution of GRB durations is bimodal, with broad peaks at  $t_{\text{GRB}} \sim 0.2$  s and  $t_{\text{GRB}} \sim 20$  s [39]. The majority of bursts belong to the long duration,  $t_{\text{GRB}} \sim 20$  s, class. The detection of afterglow emission was made possible thanks

to the accurate GRB positions provided on hour time scale by the *BeppoSAX* satellite [28]. Since the detectors on board this satellite trigger only on long bursts, afterglow observations are not available for the smaller population of short,  $t_{\text{GRB}} \sim 0.2$  s, bursts. Thus, while the discussion of the fireball model presented in §§2 and 3, based on  $\gamma$ -ray observations and on simple phenomenological arguments, applies to both long and short duration bursts, the discussion below of afterglow observations applies to long duration bursts only. It should, therefore, be kept in mind that short duration bursts may constitute a different class of GRBs which, for example, may be produced by a different class of progenitors and may have a different redshift distribution than the long duration bursts.

Afterglow observations led to the confirmation, as mentioned in §1, of the cosmological origin of GRBs [69], and supported [117,126] standard model predictions [62,80,90,112] of afterglows that result from synchrotron emission by electrons accelerated to high energy in the highly relativistic shock driven by the fireball into its surrounding gas. As discussed in separate chapters of this volume, both the spectral and temporal behavior of afterglow emission are in general agreement with model predictions.

Since afterglow emission results from the interaction of the fireball with ambient medium, it does not provide direct information on the evolution of the fireball at the earlier stage during which the GRB is produced. Nevertheless, afterglow observations may be used to indirectly test underlying model assumptions and constrain model parameters relevant for this earlier stage. We describe below several afterglow observations which have important implications for the GRB phase of the model.

#### 4.1 Fireball Size and Relativistic Expansion

Radio observations of GRB970508 allowed a direct determination of the fireball size and a direct confirmation of its relativistic expansion. As explained in §2.1, radiation seen by a distant observer originates from a conical section of the fireball around the source-observer line of sight, with opening angle  $\sim 1/\Gamma$ , and photons which are emitted from the edge of the cone are delayed compared to those emitted along the line of sight, by  $r/2\Gamma^2c$ . Thus, the apparent radius of the emitting cone is  $R = r/\Gamma(r) = 2\Gamma(r)ct$  where  $r$  and  $t$  are related by  $t = r/2\Gamma(r)^2c$ . (A detailed calculation of fireball emission introduces only a small correction,  $R = 1.9\Gamma(r)ct$  [119]. Using Eq. 15, we find that the apparent size of the fireball during its self-similar expansion into the surrounding medium is given by

$$R = 0.8 \times 10^{17} \left( \frac{1+z}{2} \right)^{-5/8} \left( \frac{E_{52}}{n_0} \right)^{1/8} \left( \frac{t}{1\text{week}} \right)^{5/8} \text{ cm}. \quad (23)$$

We have chosen here the normalization  $E = 10^{52}E_{52}$  erg since this is the energy inferred for GRB970508 [118,125] (note, however, the very weak dependence on  $E$  and  $n$ ). The factor  $1+z$  appears due to the redshift between source and observer time intervals.

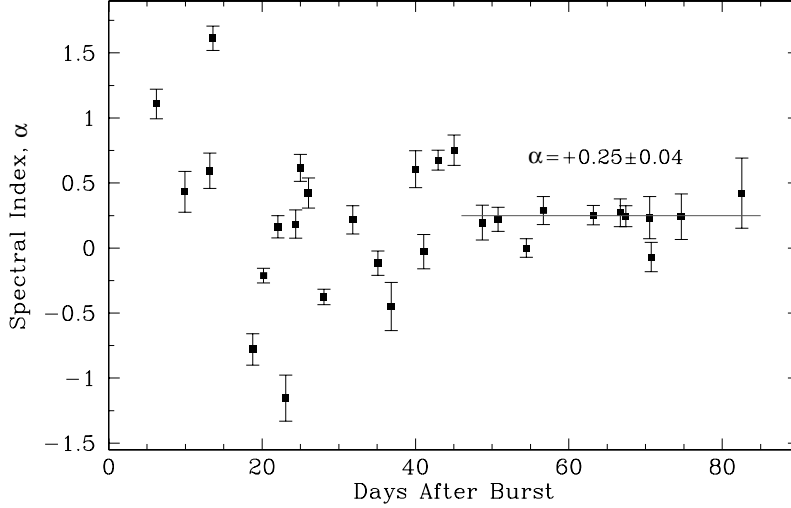


**Fig. 1.** The ratio between the GRB970508 afterglow radio fluxes at 4.86 GHz and 8.46 GHz,  $\alpha \equiv \log[f_\nu(4.86\text{GHz})/f_\nu(8.46\text{GHz})]/\log(4.86/8.46)$ , is shown as a function of time following the burst (modified from [41]). The rapid variations at early times are due to narrow band diffractive scintillation, and their quenching at late times is due to the expansion of the source beyond a critical size given by Eq. (24). This is a direct confirmation of model predictions, according to which highly relativistic plasma ejection is responsible for the observed radiation.

Scattering by irregularities in the local interstellar medium ISM may modulate the observed fireball radio flux [51]. If scattering produces multiple images of the source, interference between the multiple images may produce a diffraction pattern, leading to strong variations of the flux as the observer moves through the pattern. In order for the diffraction patterns produced by different points on the source to be similar, so that the pattern is not smoothed out due to large source size, the apparent size of a source a redshift  $z = 1$  must satisfy [125]

$$R < R_{\text{sc.}} \approx 10^{17} \frac{\nu_{10}^{6/5}}{h_{75}} \left( \frac{SM}{10^{-3.5} \text{m}^{-20/3} \text{kpc}} \right)^{-3/5} \text{ cm}, \quad (24)$$

where  $\nu = 10\nu_{10}$  GHz,  $h_{75}$  is the Hubble Constant in units of  $75 \text{ km s}^{-1} \text{ Mpc}^{-1}$ , and the scattering measure,  $SM$ , a measure of the strength of the electron density fluctuations, is normalized to its characteristic Galactic value.

Comparing Eqs. (23) and (24) we find that, on time scale of weeks, the apparent fireball size is comparable to the maximum size for which diffractive

scintillation is possible. On shorter time scales, therefore, strong modulation of the radio flux is expected, while on longer time scales we expect diffractive scintillation to be quenched. This is exactly what had been observed for GRB970508, as demonstrated in Fig. 1. Observations are therefore in agreement with fireball model predictions: They imply a source size consistent with model prediction, Eq. (23) which, in particular, imply expansion at a speed comparable to that of light.

#### 4.2 The Nature of the Fireball Plasma

Due to present technical limitations of the experiments, afterglow radiation is observed in most cases only on time scale  $\gg 10$  s. In one case, however, that of GRB990123, optical emission was detected on  $\sim 10$  s time scale [1]. The most natural explanation of the observed optical radiation is synchrotron emission from electrons accelerated to high energy in the reverse shocks driven into fireball ejecta at the onset of interaction with the surrounding medium [81,99], as explained in §3.3. This observation provides, therefore, direct constraints on the fireball ejecta plasma. First, it provides strong support for one of the underlying assumptions of the dissipative fireball scenario described in §2.2, that the energy is carried from the underlying source in the form of proton kinetic energy. This is due to the fact that the observed radiation is well accounted for in a model where a shock propagates into fireball plasma composed of protons and electrons (rather than, e.g., a pair plasma). Second, comparison of the observed flux with model predictions from Eqs. (20) and (21) implies  $\xi_e \sim \xi_B \sim 10^{-1}$ .

#### 4.3 Gamma-Ray Energy and GRB Rate

Following the determination of GRB redshifts, it is now clear that most GRB sources lie within the redshift range  $z \sim 0.5$  to  $z \sim 2$ , with some bursts observed at  $z > 3$ . For the average GRB  $\gamma$ -ray fluence,  $1.2 \times 10^{-5}$  erg  $\text{cm}^{-2}$  in the 20 keV to 2 MeV band, this implies characteristic isotropic  $\gamma$ -ray energy and luminosity  $E_\gamma \sim 10^{53}$  erg and  $L_\gamma \sim 10^{52}$  erg  $\text{s}^{-1}$  (Here, we assume a flat universe with  $\Omega = 0.3$ ,  $\Lambda = 0.7$ , and  $H_0 = 65$  km  $\text{s}^{-1}$   $\text{Mpc}^{-1}$ ). These estimates are consistent with more detailed analyses of the GRB luminosity function and redshift distribution. Mao and Mo [77], e.g., find, for the cosmological parameters we use, a median GRB energy of  $\approx 0.6 \times 10^{53}$  erg in the 50 – 300 keV band, corresponding to a median GRB energy of  $\approx 2 \times 10^{53}$  erg in the 20 keV to 2 MeV band.

Since most observed GRB sources lie within the redshift range  $z \sim 0.5 - 2$ , observations essentially determine the GRB rate per unit volume at  $z \sim 1$ . The observed rate of  $10^3$   $\text{yr}^{-1}$  implies  $R_{\text{GRB}}(z = 1) \approx 3$   $\text{Gpc}^{-3}$   $\text{yr}^{-1}$  (for  $\Omega = 0.3$ ,  $\Lambda = 0.7$ , and  $H_0 = 65$  km  $\text{s}^{-1}$   $\text{Mpc}^{-1}$ ). The present,  $z = 0$ , rate is less well constrained since available data are consistent with both no evolution of GRB rate with redshift and with strong evolution (following, e.g., the star formation rate), in which  $R_{\text{GRB}}(z = 1)/R_{\text{GRB}}(z = 0) \sim 10$  [61,68]. A detailed analysis by,

e.g., Schmidt [101] leads, assuming  $R_{\text{GRB}}$  is proportional to the star formation rate, to  $R_{\text{GRB}}(z=0) \sim 0.5 \text{ Gpc}^{-3} \text{ yr}^{-1}$ .

If fireballs are conical jets of solid angle  $\Delta\Omega$  then, clearly, the total  $\gamma$ -ray energy is smaller by a factor  $\Delta\Omega/4\pi$  than the isotropic energy, and the GRB rate is larger by the same factor.

#### 4.4 Fireball Geometry

Afterglow observations suggest that at least some GRBs are conical jets, of opening angle  $\theta \sim 10^{-1}$  corresponding to a solid angle  $\Delta\Omega \sim 10^{-2}$  [26,70,100]. As explained in §2.5, the discussion in §2 and §3 is limited to the stage where the wind is ultra-relativistic,  $\Gamma \sim 300$ , prior to significant fireball deceleration by the surrounding medium, and is hence equally valid for both a spherical and a jet-like fireball. A jet like geometry has, of course, profound implications for the underlying progenitor (see §5): it implies that the underlying source must produce a collimated outflow and, if  $\theta \sim 10^{-1}$  is indeed typical, it implies that the characteristic  $\gamma$ -ray energy emitted by the source is  $\approx 10^{51}$  erg rather than  $\approx 10^{53}$  erg implied by the assumption of isotropy.

#### 4.5 Fireball $\gamma$ -Ray Efficiency

Afterglow observations imply that a significant fraction of the energy initially carried by the fireball is converted into  $\gamma$ -rays, i.e., that the observed  $\gamma$ -ray energy provides a rough estimate of the total fireball energy. This has been demonstrated for one case, that of GRB970508, by a comparison of the total fireball energy derived from long term radio observations with the energy emitted in  $\gamma$ -rays [41,125], and for a large number of bursts by a comparison of observed  $\gamma$ -ray energy with the total fireball energy estimate based on X-ray afterglow data [42]. Freedman and Waxman [42] demonstrated that a single measurement of the X-ray afterglow flux on the time scale of a day provides a robust estimate of the fireball energy per unit solid angle,  $\varepsilon$ , averaged over a conical section of the fireball of opening angle  $\theta \sim 0.1$ . Applying their analysis to *BeppoSAX* afterglow data they demonstrated that the ratio of observed  $\gamma$ -ray to total fireball energy per unit solid angle,  $\varepsilon_\gamma/\varepsilon$ , is of order unity.

The inferred high radiative efficiency implies that a significant fraction of the wind kinetic energy must be converted to internal energy in internal shocks, and that electrons must carry a significant fraction of the internal energy, i.e., that  $\xi_e$  should be close to unity. We have already shown in §3.1 and §3.2, following [55], that efficient conversion of kinetic to internal energy and  $\xi_e$  values close to unity may naturally lead to  $\sim 1$  MeV spectral break energies, in accordance with observations.

## 5 Progenitors Clues

The observational constraints that provide the main hints regarding the nature of the underlying GRB progenitors are the rapid,  $\sim 1$  ms,  $\gamma$ -ray signal variability,

and the total  $\gamma$ -ray energy emitted by the source,  $\approx 10^{53}(\Delta\Omega/4\pi)$  erg. The rapid variability implies a compact object, of size smaller than a light millisecond,  $\sim 10^7$  cm, and mass smaller than  $\sim 30 M_\odot$  (the mass of a black hole with  $\sim 10^7$  cm Schwarzschild radius). The energy released in  $\gamma$ -rays corresponds to a  $0.1(\Delta\Omega/4\pi) M_\odot$  rest mass energy. The most natural way for triggering the GRB event is therefore the accretion of a fraction of a solar mass onto a (several) solar mass black hole (or possibly a neutron star). The dynamical time of such a source, comparable to its light crossing time, is sufficiently short to account for the observed rapid variability and, if significant fraction of the gravitational binding energy release is converted to  $\gamma$ -rays, the source will meet the observed energy requirements.

Most cosmological GRB models therefore have at their basis gravitational collapse of a several solar-mass progenitor to a black hole. Within the context of the fireball model, the observed variability is determined by the dynamical time of the source, which determines the variability in the ejected wind properties, while the GRB duration,  $\geq 10$  s for long bursts, reflects the wind duration, i.e., the duration over which energy is extracted from the source. The characteristic time for the gravitational collapse is of the order of the dynamical time, i.e., much shorter than the wind duration. Most models therefore assume that, following collapse and black hole formation, some fraction of the progenitor mass forms an accretion disk which powers the wind through gradual mass accretion. The characteristic time scale for accretion is set by the disk viscosity, which is uncertain and assumed to correspond to the observed GRB duration.

Progenitor models differ in the scenario for black hole formation, and in the process assumed to convert disk energy into relativistic outflow. The two leading progenitor scenarios are, at present, collapses of massive stars [89,128], and mergers of compact objects [50,87]. In the former case, the progenitor is a massive rotating star, e.g., a  $\sim 15 M_\odot$  helium star evolved (by mass-loss) from a  $\sim 30 M_\odot$  main sequence star. The collapse of the progenitor's  $\sim 2 M_\odot$  iron core leads to the formation of a black hole surrounded by an accretion disk composed of mantle plasma [128]. In the latter case, the merger of two neutron stars leads to the formation of a black hole surrounded by a disk produced by neutron star disruption during the merger process (see, e.g., [37]). A similar scenario involves neutron star disruption during a neutron star–black hole merger (see, e.g., [71]).

Two types of processes are widely considered for the extraction of disk energy: neutrino emission and magneto-hydrodynamic (MHD) processes. The viscous dissipation of energy, driving mass accretion, heats the dense disk plasma leading to the emission of thermal neutrinos of all flavors. Neutrino annihilation along the rotation axis in the vicinity of the black hole may then produce an electron-positron pair plasma fireball. The fraction of rest mass which is dissipated during accretion is typically of order 10% (the specific energy at the last stable orbit of a non-rotating black-hole, at three Schwarzschild radii, is  $c^2/6$ ). Accretion of  $0.1 M_\odot$  over a second may therefore lead to a neutrino luminosity of  $\approx 10^{52.5}$  erg s $^{-1}$ , of which  $\approx 1\%$  would be deposited by annihilation to drive a fireball. The resulting wind luminosity,  $\sim 10^{50}$  erg s $^{-1}$ , may be too low to



drive a spherical fireball, but may be sufficient if the fireball is collimated into  $\Delta\Omega/4\pi \sim 10^{-2}$ .

If equipartition magnetic fields,  $\sim 10^{15}$  G, are built in the disk (e.g., by convective motion) the dissipated energy may be extracted electromagnetically from the disk. Although the process by which such a strong field is generated, as well as the details of the energy extraction mechanism in the presence of such field are not understood, there is evidence from various astrophysical systems (active galactic nuclei and micro-quasars, see, e.g., [74]), for the formation of MHD driven jets which carry  $\sim 10\%$  of the disk binding energy. The presence of equipartition fields may also allow the extraction of energy directly, e.g., via the Blandford-Znajek mechanism [19], from the rotating black hole [72]. For rapid rotation, the available energy in this case is comparable to the collapsed rest mass. Thus, MHD processes are often invoked to drive a relativistic wind with efficiency much higher than that estimated for a neutrino driven wind.

We note in this context that a possible alternative to the above models may be the formation from stellar collapse of a fast rotating neutron star with ultra-high magnetic field [107,109]. If a fast rotating, millisecond period, neutron star is produced by the collapse with  $\sim 10^{15}$  G field, then the resulting electromagnetic energy luminosity is sufficient to drive a GRB wind.

One problem which all models are facing is the baryon loading. In order to allow acceleration to the high Lorentz factors implied by observations,  $\Gamma \sim 10^3$ , the total mass entrained within the expanding plasma must be smaller than  $\sim 10^{-4} M_{\odot}$ , i.e., the mass-loss rate should be smaller than  $\sim 10^{-6} M_{\odot} \text{ s}^{-1}$ . The neutrino luminosity is expected to drive mass-loss at a much higher rate. It is generally assumed that mass flow towards the rotation axis is inhibited (e.g., by high pressure of fireball plasma along the rotation axis), thus allowing the formation of a sufficiently baryon free fireball collimated along the rotation axis. In the case of a massive star progenitor, the fireball jet is assumed to form along the rotation axis of the star, where rapid rotation leads to lower mantle and envelope density. The collimation of the fireball may be due in this case to the presence of a low density funnel along the rotation axis, and the resulting jet must penetrate through the stellar mantle and envelope in order to allow the production of an observable GRB. Recent numerical and analytical calculations of the propagation of high entropy jets through stellar progenitors indicate that such a scenario may be viable [2,44,83].

Afterglow observations provide several hints which indicate that long duration GRBs, at least those for which afterglows have been detected, are associated with massive star progenitors. The location of GRBs within host galaxies, the presences of iron lines, and the evidence for a supernova association all imply massive star progenitors. Since this issue is discussed in detail in other chapters in this volume, we address it only briefly here.

Most GRB afterglows are localized within the optical image of a host galaxy [20]. This is in disagreement with simple analyses of the neutron star merger scenario which predict that the high velocity of such binaries should carry many of them outside of the host prior to merger. This result is, however, uncertain

since it depends on model parameters which are only poorly constrained, such as the distribution of initial binary separations. Evidence for the presence of iron lines has been found in X-ray data for two bursts [4,93]. While the presence of iron lines strongly suggests a massive stellar progenitor, as it indicates the presence of iron enriched environment, the confidence level of their detection is moderate. There is evidence in three cases that a supernova may be associated with the GRB [47,110]. The evidence is, however, not yet conclusive (see, e.g., [124]). Finally, the synchrotron emission produced by a shock driven by the fireball into its surrounding medium depends on the density of the ambient medium. Thus, the temporal and spectral dependence of this afterglow emission may distinguish between the high density environment characteristic of a massive stellar wind, expected to exist in the case of a massive stellar progenitor, and the low density ISM expected, e.g., in merger scenarios. Present observations are not yet conclusive, since data on time scales much shorter than one day are required to distinguish between the two cases [75].

It is clear from the above discussion, that future afterglow observations providing more detailed information on the burst environment and location will play a crucial role in placing stringent constraints on progenitor models. In addition to the points discussed in the previous paragraph, the destruction of dust [34,43,96,124] and time dependence of atomic, ionic [21,76] and molecular  $H_2$  [34,124] lines due to photoionization may be detectable for a burst in a molecular cloud environment characteristic of star forming regions.

## 6 High Energy Protons and Neutrinos from GRB Fireballs

### 6.1 Fermi Acceleration in GRBs

In the fireball model, the observed radiation is produced, both during the GRB and the afterglow, by synchrotron emission from shock accelerated electrons. In the region where electrons are accelerated, protons are also expected to be shock accelerated. This is similar to what is thought to occur in supernovae remnant shocks, where synchrotron radiation of accelerated electrons is the likely source of non-thermal X-rays (recent *Advanced Satellite for Cosmology and Astrophysics* (ASCA) observations give evidence for acceleration of electrons in the remnant of SN1006 to  $10^{14}$  eV [66]), and where shock acceleration of protons is believed to produce cosmic rays with energy extending to  $\sim 10^{15}$  eV (see, e.g., [16] for a review). Thus, it is likely that protons, as well as electrons, are accelerated to high energy within GRB fireballs.

We consider proton Fermi acceleration in fireball internal and reverse shocks (see §2.2 and §2.4 respectively). Since these shocks are mildly relativistic, with Lorentz factors  $\Gamma_i - 1 \sim 1$  in the wind frame (see §§2.4 and 3.1), the predicted energy distribution of accelerated protons is [12,16]  $dn_p/d\epsilon_p \propto \epsilon_p^{-2}$ , similar to the electron energy spectrum inferred from the observed photon spectrum.

Two constraints must be satisfied by fireball wind parameters in order to allow proton acceleration to  $\epsilon_p > 10^{20}$  eV in internal and reverse shocks. First,

the proton acceleration time,  $t_a \sim R_L/c$  where  $R_L$  is the proton Larmor radius, must be smaller than the wind expansion time [85,111,115],  $t_d \sim r_i/\Gamma c$  (in the wind frame). This constraint sets a lower limit to the magnetic field carried by the wind, which may be expressed as [115]:

$$\xi_B/\xi_e > 0.02\Gamma_{2.5}^2\epsilon_{p,20}^2L_{\gamma,52}^{-1}. \quad (25)$$

Here,  $\epsilon_p = 10^{20}\epsilon_{p,20}$  eV. Recall that  $\xi_B$  is the fraction of the wind energy density which is carried by magnetic field,  $4\pi r^2 c\Gamma^2(B^2/8\pi) = \xi_B L$ , and  $\xi_e$  is the fraction of wind energy carried by shock accelerated electrons. Since the electron energy is lost radiatively,  $L_\gamma \approx \xi_e L$ .

The second constraint that should be satisfied is that the proton synchrotron loss time must exceed  $t_a$ , setting an upper limit to the magnetic field. The latter constraint may be satisfied simultaneously with the lower limit to the magnetic field, Eq. (25), provided [115]

$$\Gamma > 130\epsilon_{p,20}^{3/4}\Delta t_{-2}^{-1/4}. \quad (26)$$

The constraints that must be satisfied to allow acceleration of protons to energy  $> 10^{20}$  eV are remarkably similar to those inferred from  $\gamma$ -ray observations:  $\Gamma > 100$  is implied by observed  $\gamma$ -ray spectra (see §§2.1 and 2.3), and magnetic field close to equipartition,  $\xi_B \sim 1$ , is required in order for electron synchrotron emission to account for the observed radiation (see §3.1).

It has recently been claimed [48] that the conditions at the external shock driven by the fireball into the ambient gas are not likely to allow proton acceleration to ultra-high energy. Regardless of the validity of this claim, it is irrelevant for the acceleration in internal shocks, the scenario considered for UHECR production in GRBs [111,115]. Moreover, it is not at all clear that UHECRs cannot be produced at the external shock, since the magnetic field may be amplified ahead of the shock by the streaming of high energy particles. For discussion of high energy proton production in the external shock and its possible implications see Dermer [33].

## 6.2 UHECR Flux and Spectrum

The local ( $z = 0$ ) energy production rate in  $\gamma$ -rays by GRBs is roughly given by the product of the characteristic GRB  $\gamma$ -ray energy,  $E \approx 2 \times 10^{53}$  erg, and the local GRB rate. Under the assumption that the GRB rate evolution is similar to the star-formation rate evolution, the local GRB rate is  $\sim 0.5 \text{ Gpc}^{-3} \text{ yr}^{-1}$  [101] (see §4.3), implying a local  $\gamma$ -ray energy generation rate of  $\approx 10^{44} \text{ erg Mpc}^{-3} \text{ yr}^{-1}$ . The energy observed in  $\gamma$ -rays reflects the fireball energy in accelerated electrons. Thus, if accelerated electrons and protons carry similar energy (as indicated by afterglow observations [42] (see, however, [108]) then the GRB production rate of high energy protons is

$$\epsilon_p^2(d\dot{n}_p/d\epsilon_p)_{z=0} \approx 10^{44} \text{ erg Mpc}^{-3} \text{ yr}^{-1}. \quad (27)$$

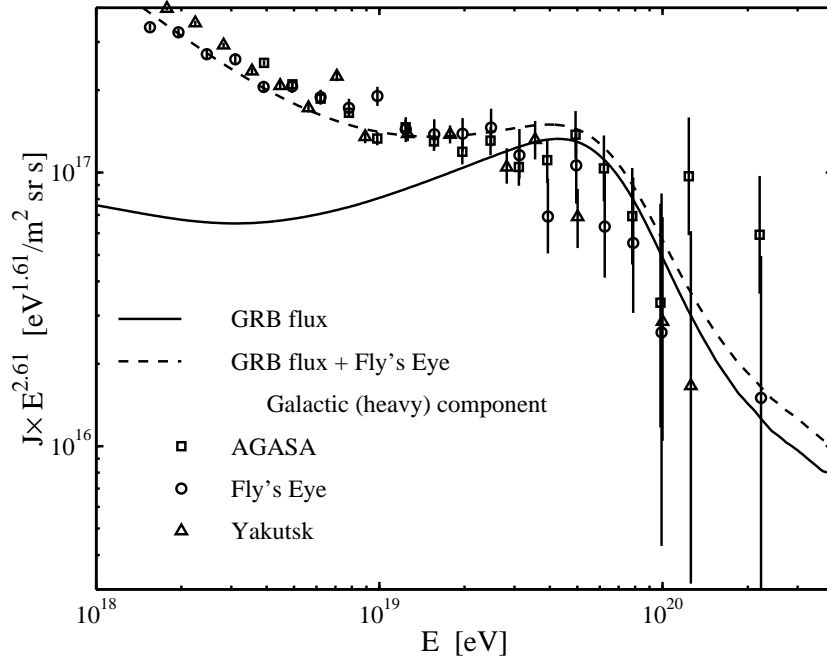


**Fig. 2.** The UHECR flux expected in a cosmological model where high-energy protons are produced at a rate  $(\epsilon_p^2 d\dot{n}_p/d\epsilon_p)_{z=0} = 0.8 \times 10^{44} \text{ erg Mpc}^{-3} \text{ yr}^{-1}$  as predicted in the GRB model (Eq. 27, solid line), compared to the *High Resolution Fly's Eye (HiRes)* [15], *Yakutsk Extensive Air Shower Array (Yakutsk)* [35] and *Akeno Giant Air Shower Array (AGASA)* [105] data.  $1\sigma$  flux error bars are shown. The dashed line is the sum of the GRB model flux and the *HiRes* fit (with normalization increased by 25%) to the Galactic heavy nuclei component [15],  $J_G \propto E^{-3.5}$ , which dominates below  $\sim 10^{19}$  eV.

In Fig. 2 we compare the observed UHECR spectrum with that predicted by the GRB model. The generation rate (Eq. 27) of high energy protons is remarkably similar to that required to account for the flux of  $> 10^{19}$  eV cosmic-rays. The flux at lower energies is most likely dominated by heavy nuclei of Galactic origin [15], as indicated by the flattening of the spectrum at  $\approx 10^{19}$  eV and by the evidence for a change in composition at this energy [14,15,31,46,113].

The suppression of model flux above  $10^{19.7}$  eV is due to energy loss of high energy protons in interaction with the microwave background, i.e., to the “GZK cutoff” [52,129]. The available data do not allow determination of the existence (or absence) of the “cutoff” with high confidence. The *Akeno Giant Air Shower Array (AGASA)* results show an excess ( $\sim 2.5\sigma$  confidence level) of events compared to model predictions above  $10^{20}$  eV. This excess is not confirmed, however, by other experiments. Moreover, since the  $10^{20}$  eV flux is dominated by sources at distances  $< 100$  Mpc, over which the distribution of known astrophysical systems (e.g., galaxies and clusters of galaxies) is inhomogeneous, significant

deviations from model predictions presented in Fig. 1 for a uniform source distribution are expected [116]. Clustering of cosmic-ray sources leads to a standard deviation,  $\sigma$ , in the expected number,  $N$ , of events above  $10^{20}$  eV given by [8]

$$\sigma/N = 0.9(d_0/10\text{Mpc})^{0.9}, \quad (28)$$

where  $d_0$  is the unknown scale length of the source correlation function and  $d_0 \sim 10$  Mpc for field galaxies.

Although the rate of GRBs out to a distance of 100 Mpc from Earth, the maximum distance traveled by  $> 10^{20}$  eV protons, is in the range of  $10^{-2}$  to  $10^{-3}$  yr, the number of different GRBs contributing to the flux of  $> 10^{20}$  eV protons at any given time may be large. This is due to the dispersion,  $\Delta t$ , in proton arrival time, which is expected due to deflection by intergalactic magnetic fields and may be as large as  $10^7$  yr. This implies that the number of sources contributing to the flux at any given time may be as large as [115]  $\sim \Delta t \times 10^{-3}$  yr  $\sim 10^4$ .

### 6.3 Neutrino Production

A burst of  $\sim 10^{14}$  eV neutrinos accompanying observed  $\gamma$ -rays is a natural consequence of the conventional fireball scenario [122]. The neutrinos are produced by  $\pi^+$  created in interactions between fireball  $\gamma$ -rays and accelerated protons. The key relation is between the observed photon energy,  $\epsilon_\gamma$ , and the accelerated proton's energy,  $\epsilon_p$ , at the photo-meson threshold of the  $\Delta$ -resonance. In the observer frame,

$$\epsilon_\gamma \epsilon_p = 0.2 \Gamma^2 \text{ GeV}^2. \quad (29)$$

For  $\Gamma \approx 300$  and  $\epsilon_\gamma = 1$  MeV, we see that characteristic proton energies  $\sim 10^{16}$  eV are required to produce pions. The pion typically carries  $\approx 20\%$  of the interacting proton energy, and this energy is roughly equally distributed between the leptons in the decay  $\pi^+ \rightarrow \mu^+ + \nu_\mu \rightarrow e^+ + \nu_e + \bar{\nu}_\mu + \nu_\mu$ . Thus, proton interaction with fireball  $\gamma$ -rays is expected to produce  $\sim 10^{14}$  eV neutrinos.

The fraction  $f_\pi(\epsilon_p)$  of proton energy lost to pion production is determined by the number density of photons in the dissipation region and is  $\approx 20\%$  at high proton energy for fireball wind parameters implied by  $\gamma$ -ray observations [56,122]. Assuming that GRBs produce high energy protons at a rate given by Eq. (27), the intensity of high energy neutrinos is [122]

$$\epsilon_\nu^2 \Phi_{\nu_x} \approx 10^{-9} \left( \frac{f_\pi}{0.2} \right) \min \left( 1, \frac{\epsilon_\nu}{10^{14}\text{eV}} \right) \text{ GeV cm}^{-2} \text{ sr}^{-1} \text{ s}^{-1}. \quad (30)$$

Here,  $\nu_x$  stands for  $\nu_\mu$ ,  $\bar{\nu}_\mu$  or  $\nu_e$ . The neutrino flux of Eq. (30) is suppressed at high energy,  $> 10^{16}$  eV, due to synchrotron energy loss of pions and muons [94,122].

During the transition to self-similarity, high energy protons accelerated in the reverse shock may interact with the 10 eV to 1 keV photons radiated by the

accelerated electrons to produce, through pion decay, a burst of duration  $\sim t_\pi$  of ultra-high energy,  $10^{17} - 10^{19}$  eV, neutrinos [123] as indicated by Eq. (29). The flux of these neutrinos depends on the density of gas surrounding the fireball. It is weak, and undetectable by experiments under construction, if the density is  $n \sim 1 \text{ cm}^{-3}$ , a value typical for the ISM. If GRBs result, however, from the collapse of massive stars, then the fireball is expected to expand into a pre-existing wind and the transition to self-similar behavior takes place at a radius where the wind density is  $n \approx 10^4 \text{ cm}^{-3} \gg 1 \text{ cm}^{-3}$ . In this case, a typical GRB at  $z \sim 1$  is expected to produce a neutrino fluence [30,123]

$$\epsilon_\nu^2 \Phi_{\nu_x} \approx 10^{-2.5} \left( \frac{\epsilon_\nu}{10^{17} \text{eV}} \right)^\alpha \text{ GeV cm}^{-2}, \quad (31)$$

where  $\alpha = 0$  for  $\epsilon_\nu > 10^{17} \text{eV}$  and  $\alpha = 1$  for  $\epsilon_\nu < 10^{17} \text{eV}$ . The neutrino flux is expected to be strongly suppressed at energy  $> 10^{19}$  eV, since protons are not expected to be accelerated to energy  $\gg 10^{20}$  eV.

#### 6.4 Implications of Neutrino Emission

The predicted intensity of  $10^{14}$  eV neutrinos produced by photo-meson interactions with observed 1 MeV photons, Eq. (30), implies a detection of  $\sim 10$  neutrino induced muons per year in planned  $1 \text{ km}^3$  Čerenkov neutrino detectors, correlated in time and direction with GRBs [3,58,122]. The predicted intensity of  $10^{17}$  eV neutrinos, produced by photo-meson interactions during the onset of fireball interaction with its surrounding medium in the case of fireball expansion into a pre-existing wind, Eq. (31), implies a detection of several neutrino induced muons per year in a  $1 \text{ km}^3$  detector. In this case, the predicted flux of  $10^{19}$  eV neutrinos may also be detectable by planned large air-shower detectors [23,73,104].

Detection of high energy neutrinos will test the shock acceleration mechanism and the suggestion that GRBs are the sources of ultra-high energy protons, since  $\geq 10^{14}$  eV ( $\geq 10^{18}$  eV) neutrino production requires protons of energy  $\geq 10^{16}$  eV ( $\geq 10^{19}$  eV). The dependence of the  $\sim 10^{17}$  eV neutrino flux on fireball environment implies that the detection of high energy neutrinos will also provide constraints on the GRB progenitors. Furthermore, it has recently been pointed out [84] that if GRBs originate from core-collapse of massive stars, then a burst of  $\geq 5$  TeV neutrinos may be produced by photo-meson interaction while the jet propagates through the envelope, with TeV fluence implying 0.1 – 10 neutrino events per individual collapse in a  $1 \text{ km}^3$  neutrino telescope. (The neutrino flux which may result from nuclear collisions in the expanding jet is more difficult to detect due to the low energy of neutrinos,  $\sim 10$  GeV, produced by this process [7,32,82]).

Detection of neutrinos from GRBs could be used to test the simultaneity of neutrino and photon arrival to an accuracy of  $\sim 1$  s ( $\sim 1$  ms for short bursts), checking the assumption of special relativity that photons and neutrinos have the same limiting speed. These observations would also test the weak equivalence principle, according to which photons and neutrinos should suffer the same time

delay as they pass through a gravitational potential. With 1 s accuracy, a burst at 100 Mpc would reveal a fractional difference in limiting speed of  $10^{-16}$ , and a fractional difference in gravitational time delay of order  $10^{-6}$  (considering the Galactic potential alone). Previous applications of these ideas to SN1987A, where simultaneity could be checked only to an accuracy of order several hours, yielded much weaker upper limits, of order  $10^{-8}$  and  $10^{-2}$  for fractional differences in the limiting speed and time delay respectively [6].

The model discussed above predicts the production of high energy muon and electron neutrinos. However, if the atmospheric neutrino anomaly has the explanation usually given [25,40,45], oscillation to  $\nu_\tau$ 's with mass  $\sim 0.1$  eV, then one should detect equal numbers of  $\nu_\mu$ 's and  $\nu_\tau$ 's. Up-going  $\tau$ 's, rather than  $\mu$ 's, would be a distinctive signature of such oscillations. Since  $\nu_\tau$ 's are not expected to be produced in the fireball, looking for  $\tau$ 's would be an "appearance experiment." To allow flavor change, the difference in squared neutrino masses,  $\Delta m^2$ , should exceed a minimum value proportional to the ratio of source distance and neutrino energy [6]. A burst at 100 Mpc producing  $10^{14}$  eV neutrinos can test for  $\Delta m^2 \geq 10^{-16}$  eV<sup>2</sup>, 5 orders of magnitude more sensitive than solar neutrinos.

### Acknowledgments

This work was supported in part by grants from the Israel-US BSF (BSF-9800343), MINERVA, and AEC (AEC-38/99). EW is the Incumbent of the Beracha foundation career development chair.

### References

1. C.W. Akerlof et al.: Nature **398**, 400 (1999)
2. M. Aloy et al.: Astrophys. J. Lett. **531**, L119 (2000)
3. J. Alvarez-Muniz, F. Halzen, D.W. Hooper: Phys. Rev. **D62**, 093015 (2000)
4. L. Amati et al.: Science **290**, 953 (2000)
5. W.I. Axford, E. Leer, E., G. Skadron: In: *Proc. 15th Internat. Cosmic Ray Conference at Plovdiv, Bulgaria, August 13-26, 1977* (B'lgarska Akademia na Naukite, Sofia 1978) p. 132
6. J.N. Bahcall: In: *Neutrino Astrophysics* (Cambridge University Press, Cambridge 1989) p. 438
7. J.N. Bahcall, P. Mészáros: Phys. Rev. Lett. **85**, 1362 (2000)
8. J.N. Bahcall, E. Waxman: Astrophys. J. **542**, 542 (2000)
9. D. Band et al.: Astrophys. J. **413**, 281 (1993)
10. M. Baring: Astrophys. J. **418**, 391 (1993)
11. J. Bednarz, M. Ostrowski: Phys. Rev. Lett. **80**, 3911 (1998)
12. A.R. Bell: Mon. Not. R. Astron. Soc. **182**, 147 (1978)
13. P.N. Bhat et al.: Nature **359**, 217 (1992)
14. D.J. Bird et al.: Phys. Rev. Lett. **71**, 3401 (1993)
15. D.J. Bird et al.: Astrophys. J. **424**, 491 (1994)
16. R. Blandford, D. Eichler: Phys. Rep. **154**, 1 (1987)
17. R.D. Blandford, C.F. Mckee: Phys. Fluids **19**, 1130 (1976)

18. R.D. Blandford, J.P. Ostriker: *Astrophys. J. Lett.* **221**, L229 (1978)
19. R.D. Blandford, R.L. Znajek: *Mon. Not. R. Astron. Soc.* **179**, 433 (1977)
20. J.S. Bloom, S.R. Kulkarni, S.G. Djorgovski: *Astron. J.* **123**, 1111 (2002)
21. M. Böttcher, C.D. Dermer, E.P. Liang: *Astron. Astrophys. Suppl. Ser.* **138**, 343 (1999)
22. J.J. Brainerd et al.: In: *Proc. 19th Texas Symposium on Relativistic Astrophysics and Cosmology at Paris, France, December 14–18, 1998*, ed. J. Paul, T. Montmerle, E. Aubourg (CEA, Saclay 1998)
23. K.S. Capelle, J.W. Cronin, G. Parente, E. Zas: *Astropart. Phys.* **8**, 321 (1998)
24. P.J. Cargill, K. Papadopoulos: *Astrophys. J. Lett.* **329**, L29 (1988)
25. D. Casper et al.: *Phys. Rev. Lett.* **66**, 2561 (1991)
26. A.J. Castro-Tirado et al.: *Science* **283**, 2069 (1999)
27. S.C. Corbató et al.: *Nucl. Phys. B* **28B**, 36 (1992)
28. E. Costa et al.: *Nature* **387**, 783 (1997)
29. J.W. Cronin: *Nucl. Phys. B* **28B**, 213 (1992)
30. Z.G. Dai, T. Lu: *Astrophys. J.* **551**, 249 (2001)
31. B.R. Dawson, R. Meyhandan, K.M. Simpson: *Astropart. Phys.* **9**, 331 (1998)
32. E.V. Derishev, V.V. Kocharovsky, V.I. Kocharovsky: *Astrophys. J.* **521**, 640 (1999)
33. C.D. Dermer: *Astrophys. J.* **574**, 65 (2002)
34. T.D. Draine, L. Hao: *Astrophys. J.* **569**, 780 (2002)
35. N.N. Efimov et al.: In: *Proc. of the Internat. Symp. on Astrophys. Aspects of the Most Energetic Cosmic-Rays*, ed. by M. Nagano, F. Takahara (World Scientific, Singapore 1991) p. 20
36. D. Eichler, A. Levinson: *Astrophys. J.* **529**, 146 (2000)
37. D. Eichler, M. Livio, D.N. Schramm: *Nature* **340**, 126 (1989)
38. G.J. Fishman et al.: *Astrophys. J. Suppl.* **92**, 229 (1994)
39. G.J. Fishman, C.A. Meegan: *Ann. Rev. Astron. Astrophys.* **33**, 415 (1995)
40. G.L. Fogli, E. Lisi: *Phys. Rev.* **D52**, 2775 (1995)
41. D. Frail, E. Waxman, S. Kulkarni: *Astrophys. J.* **537**, 191 (2000)
42. D.L. Freedman, E. Waxman: *Astrophys. J.* **547**, 922 (2001)
43. A.S. Fruchter, J.H. Krolik, J.E. Rhoads: *Astrophys. J.* **563**, 597 (2001)
44. C.L. Fryer, S.E. Woosley: *Astrophys. J. Lett.* **502**, L9 (1998)
45. Y. Fukuda et al.: *Mod. Phys. Lett. B* **B335**, 237 (1994)
46. T.K. Gaisser et al.: *Phys. Rev.* **D47**, 1919 (1993)
47. T. Galama et al.: *Nature* **395**, 670 (1998)
48. Y.A. Gallant, A. Achterberg: *Mon. Not. R. Astron. Soc.* **305**, L6 (1999)
49. G. Ghisellini, A. Celotti: *Astrophys. J. Lett.* **511**, L93 (1999)
50. J. Goodman: *Astrophys. J. Lett.* **308**, L47 (1986)
51. J. Goodman: *New Astron.* **2**, 449 (1997)
52. K. Greisen: *Phys. Rev. Lett.* **16**, 748 (1966)
53. A. Gruzinov, E. Waxman: *Astrophys. J.* **511**, 852 (1999)
54. A. Gruzinov: *Astrophys. J.* **563**, 15 (2001)
55. D. Guetta, M. Spada, E. Waxman: *Astrophys. J.* **557**, 399 (2001)
56. D. Guetta, M. Spada, E. Waxman: *Astrophys. J.* **559**, 101 (2001)
57. F. Halzen: In: *Weak Interactions and Neutrinos, Proc. of the 17th Internat. Workshop at Cape Town, South Africa, January 24–30, 1999*, ed. by C.A. Dominguez, R.D. Viollier (World Scientific Publishers, Singapore 2000) p. 123
58. F. Halzen, D.W. Hooper: *Astrophys. J. Lett.* **527**, L93 (1999)



59. N. Hayashida et al.: *Astrophys. J.* **522**, 225 (1999)
60. D.J. Helfand, R.H. Becker: *Astrophys. J.* **314**, 203 (1987)
61. D.W. Hogg, A.S. Fruchter: *Astrophys. J.* **520**, 54 (1999)
62. J.I. Katz: *Astrophys. J. Lett.* **432**, L107 (1994)
63. Y. Kazimura, J.I. Sakai, T. Neubert, S.V. Bulanov: *Astrophys. J. Lett.* **498**, L183 (1998)
64. R.M. Kippen: In: *Gamma-Ray Bursts in the Afterglow Era, Proc. International Workshop at Rome, Italy, 17–20 October 2000*, ed. by E. Costa, F. Frontera, J. Hjorth (Springer, Heidelberg 2001)
65. J.G. Kirk, A.W. Guthmann, Y.A. Gallant, A. Achterberg: *Astrophys. J.* **542**, 235 (2000)
66. K. Koyama et al.: *Nature* **378**, 255 (1995)
67. J.H. Krolik, E.A. Pier: *Astrophys. J.* **373**, 277 (1991)
68. M. Krumholtz, S.E. Thorsett, F.A. Harrison: *Astrophys. J. Lett.* **506**, L81 (1998)
69. S.R. Kulkarni et al.: *SPIE* **4005**, 9 (2000)
70. S.R. Kulkarni et al.: *Nature* **398**, 389 (1999)
71. J.M. Lattimer, D.N. Schramm: *Astrophys. J. Lett.* **192**, L145 (1974)
72. A. Levinson, D. Eichler: *Astrophys. J.* **418**, 386 (1993)
73. J. Linsley: In: *Proc. 19th Internat. Cosmic Ray Conference at La Jolla, CA, USA, August 11–23, 1985*, ed. by F.C. Jones et al. (NASA Conf. Publ. No. 2376, 1985) p. 438
74. M. Livio: *Phys. Rep.* **311**, 225 (1999)
75. M. Livio, E. Waxman: *Astrophys. J.* **538**, 187 (2000)
76. A. Loeb, R. Perna: *Astrophys. J. Lett.* **503**, L35 (1998)
77. S. Mao, H.J. Mo: *Astron. Astrophys.* **339**, L1 (1998)
78. P. Mészáros: *Astron. Astrophys. Suppl. Ser.* **138**, 533 (1999)
79. P. Mészáros, M. Rees: *Mon. Not. R. Astron. Soc.* **269**, 41P (1994)
80. P. Mészáros, M. Rees: *Astrophys. J.* **476**, 232 (1997)
81. P. Mészáros, M. Rees: *Mon. Not. R. Astron. Soc.* **306**, L39 (1999)
82. P. Mészáros, M. Rees: *Astrophys. J. Lett.* **541**, L5 (2000)
83. P. Mészáros, M. Rees: *Astrophys. J.* **556**, 37 (2001)
84. P. Mészáros, E. Waxman: *Phys. Rev. Lett.* **87**, 1101 (2001)
85. M. Milgrom, V. Usov: *Astrophys. J. Lett.* **449**, L37 (1995)
86. R. Narayan, B. Paczyński, T. Piran: *Astrophys. J. Lett.* **395**, L83 (1992)
87. B. Paczyński: *Astrophys. J. Lett.* **308**, L43 (1986)
88. B. Paczyński: *Astrophys. J.* **363**, 218 (1990)
89. B. Paczyński: In: *Gamma-Ray Bursts, 4th Huntsville Symposium at Huntsville, AL, USA, September 15–20, 1997*, ed. by C. Meegan, R. Preece, T. Koshut (AIP Press, New York 1998), p.783
90. B. Paczyński, J. Rhoads: *Astrophys. J. Lett.* **418**, L5 (1993)
91. B. Paczyński, G. Xu: *Astrophys. J.* **427**, 708 (1994)
92. T. Piran: *Phys. Rep.* **333**, 529 (2000)
93. L. Piro et al.: *Science* **290**, 955 (2000)
94. J.P. Rachen, P. Mészáros: *Phys. Rev. D* **58**, 123005 (1998)
95. M. Rees, P. Mészáros: *Mon. Not. R. Astron. Soc.* **258**, 41P (1992)
96. D.E. Reichart: *astro-ph* 0107546 (2001)
97. R.Z. Sagdeev: *Rev. Plasma Phys.* **4**, 23 (1966)
98. R. Sari, T. Piran: *Astrophys. J.* **485**, 270 (1997)
99. R. Sari, T. Piran: *Astrophys. J. Lett.* **517**, L109 (1999)
100. R. Sari, T. Piran, J. Halpern: *Astrophys. J. Lett.* **519**, L17 (1999)

101. M. Schmidt: *Astrophys. J.* **552**, 36 (2001)
102. A. Shemi, T. Piran: *Astrophys. J. Lett.* **365**, L55 (1990)
103. M. Sommer et al.: *Astrophys. J. Lett.* **422**, L63 (1994)
104. Y. Takahashi: In: *Proc. 24th Internat. Cosmic-Ray Conference at Rome, Italy, August 28–September 8, 1995*, ed. by N. Iucci, E. Lamanna (XXIV ICRC, Rome 1995) p. 595
105. M. Takeda et al.: *Phys. Rev. Lett.* **81**, 1163 (1998)
106. M. Teshima et al.: *Nucl. Phys. B* **28B**, 169 (1992)
107. C. Thompson: *Mon. Not. R. Astron. Soc.* **270**, 480 (1994)
108. T. Totani: *Astron. Astrophys. Suppl. Ser.* **142**, 443 (2000)
109. V.V. Usov: *Mon. Not. R. Astron. Soc.* **267**, 1035 (1994)
110. J. van Paradijs et al.: *Science* **286**, 693 (1999)
111. M. Vietri: *Astrophys. J.* **453**, 883 (1995)
112. M. Vietri: *Astrophys. J. Lett.* **478**, L9 (1997)
113. A.A. Watson: *Nucl. Phys. B* **22B**, 116 (1991)
114. A.A. Watson: In: *Nuclear and Particle Physics, Inst. of Physics Conf. Series*, ed. I.J.D. MacGregor, A.T. Doyle (IoP, Bristol 1993) p. 135
115. E. Waxman: *Phys. Rev. Lett.* **75**, 386 (1995)
116. E. Waxman: *Astrophys. J. Lett.* **452**, L1 (1995)
117. E. Waxman: *Astrophys. J. Lett.* **485**, L5 (1997)
118. E. Waxman: *Astrophys. J. Lett.* **489**, L33 (1997)
119. E. Waxman: *Astrophys. J. Lett.* **491**, L19 (1997)
120. E. Waxman: *Nucl. Phys. B* **87**, 345 (2000)
121. E. Waxman: In: *ICTP Summer School at ICTP, Italy, June 2000 and VI Gleb Wataghin School at UNICAMP, Brazil, July 2000*, Lecture Notes (astro-ph/0103186)
122. E. Waxman, J.N. Bahcall: *Phys. Rev. Lett.* **78**, 2292 (1997)
123. E. Waxman, N.J. Bahcall: *Astrophys. J.* **541**, 707 (2000)
124. E. Waxman, B.T. Draine: *Astrophys. J.* **537**, 796 (2000)
125. E. Waxman, S. Kulkarni, D. Frail: *Astrophys. J.* **497**, 288 (1998)
126. A.M.J. Wijers, M.J. Rees, P. Mészáros: *Mon. Not. R. Astron. Soc.* **288**, L51 (1997)
127. E. Woods, A. Loeb: *Astrophys. J.* **453**, 583 (1995)
128. S.E. Woosley: *Astrophys. J.* **405**, 273 (1993)
129. G.T. Zatsepin, V.A. Kuzmin: *JETP Lett.* **4**, 78 (1966)